Earthquake Engineering, Tenth World Conference © 1992 Balkema, Rotterdam. ISBN 90 5410 060 5

# Directional behavior of strong ground motions during the Loma Prieta earthquake

T. Kaneko & T. Mikami
*Hokkaido College, Senshu University, Bibai, Japan*

T. Hayashikawa
*Hokkaido University, Sapporo, Japan*

Y. Matsui
*Chuoh Consultants Co., Ltd, Sapporo, Japan*

ABSTRACT: Records of the Loma Prieta Earthquake which were published at the USGS and CDMG in California on the wave form analysis of the strong motion seismograms are selected. The directional behavior and the rectilinear characteristics of the ground motion were investigated with the focus of attention on the direction of the principal axis and values of the rectilinearity. These were analyzed with special care. The three components of the main axis are taken into consideration and the rectilinearity formula is proposed. The maximal acceleration of the direction of the major principal axis is calculated and the results are compared with the maximal acceleration of the original seismograms.

## 1 INTRODUCTION

The Loma Prieta Earthquake(October 17th, 1989) was caused by a slip in the San Andreas Fault brought about by a shift of 1.3 m upwards and 1.9 m north west of the Pacific Plate against the North American Plate. It is of considerable interest to follow the main shock caused by the slip to the north of San Francisco Bay area, to the south of Monterey, to the east of Walls Valley, further it is of interest to know what vibrations exceed. Strong motion seismograms among the ground motion observed throughout Loma Prieta Earthquake in San Francisco Bay Area will be widely utilized from a stand point of civil engineering. For this reason wave form analysis of strong motion seismograms are conducted. It is necessary to accurately grasp the characteristics of ground motion and various workers have attempted an effective wave form analyses.

In this paper, digital data of records were published at the USGS(United States Geological Survey) and the CDMG(California Department of Conservation, Division of Mines and Geology) on three dimentional wave form analysis of these strong motion seismograms are selected. Polarization analysis are madé on three component acceleration records.

The plastic polarization filter techniques applied on the time domain used here is set forth by E.A.Flinn (1965). One of these the Rectilinear Motion Detecter Filter analysis is widely used by researchers to emphasize the phase difference that points in the direction of the seismic wave. In the seismic wave analysis of the actual earthquake, the separation of the P waves and S waves that originated at the seismic source and the following waves that arose from the refraction and reflection of the body waves by the boundary layers or the irreguler ground layers are the main purposes of this application.
In addition the polarization filter technique is used for the separation of back ground noise such as microtremors, or adjudgement of recent multiple shocks and differentiation of body waves and surface waves. In any event the accumulation of knowledge of filter analysis is growing. The characteristics of this analytical method are expressed by the dual parameters of the rectilinearity of the elliptic, particle orbital motion in a three dimensional space and in the direction of polarization.

Here, the state of polarization of seismic motion is surmised from the three component acceleration seismic records and seperation of principal component waves are conducted.

In addition, this is advanced to the synthesis of waves in the direction of the major axis in the main quake motion which showed maximum power of the principal component wave. As a result, from this three component strong motion records a major axis segregated wave is synthesized which could be utilized as a more practical means for earthquake resistant design input waves for structure. This could be applied for practical purposes engineering-wise.

## 2 POLARIZATION FILTER ANALYSIS

Regarding the polarization analysis of strong motion earthquake records the idea is based on J.F. Montalbetti et al(1970) method, the actual work is done as indicated in the order of Figure 1; the flow chart is handled in the order of the flow. The explanation of the

analysis will be made in that order.

[1] The necessary digital data is lead forth from the data base of the three component acceleration strong motion seismograms.

[2] Among the three component seismogram GB1, when the horizontal component is not in the direction of NS, EW, the component is constructed by co-ordinate exchange to NS, EW component is $G_i$. Here in a sense of grasping the characteristics as a whole of the entire seismic motion, 2 out of the 3 components, namely NS and EW, then NS and UD, EW and UD are paired, and the orbit spectrum is drawn by seismic particle motion for each frequency and each time for the purpose of utilization.

[3] The seismic waves are divided into M sections and the covariance matrix regarding the digital volume of N number in the first section was calculated.

$$V = \begin{pmatrix} \mathrm{Var}[G_{NS}] & \mathrm{Cov}[G_{NS}, G_{EW}] & \mathrm{Cov}[G_{NS}, G_{UD}] \\ \mathrm{Cov}[G_{NS}, G_{EW}] & \mathrm{Var}[G_{EW}] & \mathrm{Cov}[G_{EW}, G_{UD}] \\ \mathrm{Cov}[G_{NS}, G_{UD}] & \mathrm{Cov}[G_{EW}, G_{UD}] & \mathrm{Var}[G_{UD}] \end{pmatrix} \quad \cdots\cdots\cdots\cdots\cdots\cdots (1)$$

[4] The eigen value and eigen vector of the determinant is calculated and from these values the size of this major axis, intermediate axis, and minor axis ($\lambda_i$), their respective incident angle ($\phi_i$) and direction angle ($\theta_i$) are calculated and the time difference of dispersion size are depicted in figures. Here the i=1, 2, 3.

[5] From direction angle and incident angle with the attention on basic horizontal direction component R(radial) and component T at right angle to the direction (transverse) and the upward and downward direction Z(vertical), the direction function which synthesizes the waves consisting of these three components

$$D_i = (e_i)^k, \quad i=R, T, Z, \quad \cdots\cdots\cdots (2)$$

are calculated. Further, $e_i$ is the function of the change of direction co-ordinates for instance the related expression of the changes of co-ordinates in the horizontal direction can be written as follows,

$$\left.\begin{aligned} e_R &= X = x\cos\theta + y\sin\theta \\ e_T &= Y = y\cos\theta - x\sin\theta \end{aligned}\right\} \quad \cdots\cdots (3)$$

Further with regard to the Rectilinearity Function in the case of two dimensions used by Flinn

$$F_1 = \left\{1 - \left(\frac{\lambda_1}{\lambda_2}\right)^n\right\}^m \quad \cdots\cdots\cdots (4)$$

expanding this to three dimensions, we have

$$F_2 = \left\{1 - \left(\frac{\lambda_2^2 + \lambda_2\lambda_3 + \lambda_3^2}{3\lambda_1^2}\right)^n\right\}^m \quad \cdots (5)$$

he defines this in the above manner. Here, the clause within the bracket of expression (5) the surface area of the oval made by the principal axis

$A_1 = \pi\lambda_1\lambda_2$, $A_2 = \pi\lambda_1\lambda_3$, $A_3 = \pi\lambda_2\lambda_3$

the cubic volume of oval sphere

$V = 4\pi\lambda_1\lambda_2\lambda_3/3$

the surface area of the circle with the maximum principal radius

$A = \pi\lambda_1^2$

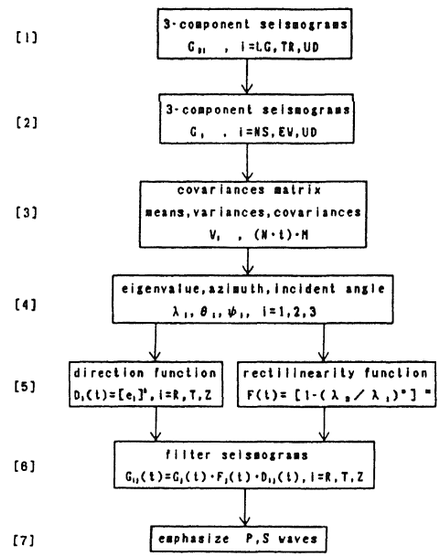


Figure 1. A flow chart of the polarization analysis.

the cubic volume

$V = 4\pi\lambda_1^3/3$

ratio are respectively combined and used.

In all cases the values are taken between 0 and 1, where the motion is confined in a circle $F_1=0$, where the motion is confined in a sphere $F_2=0$ (in extreme cases). And when the value becomes 1 both $F_1$ and $F_2$ has a sway vibration. In $F_2$ when a circular plate motion is achieved, the values stand at 2/3.

Further, in cases herein after the analytical cases uses k=2, n=1, m=1. These N numbers of digital data(when the data space is t seconds N·t seconds in time) corresponds to sumarize the calculations in the first section and is a linear time window function.

In order to apply this to all seismic waves, the window time space is rendered constant and the center of the window time $t_j$ (j=1, 2, ····M) is a filter function and the time is renewed in the respective order and the same calculations are repeated. As a result of the time shift, the window changes M times, hence it can be considered as a plastic filter and in this case the adjacent windows is said to have superimposed time filters.

This can be considered when a low pass filter is applied (Figure 2. transformation of the

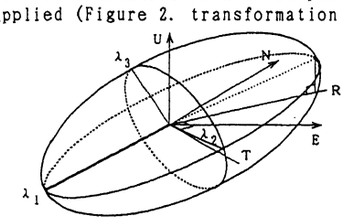


Figure 2. Transformation of the azimuth and principal axis.

azimuth and principal axes).

[6] In the final analysis, the seismic wave form $GM_i$ which places emphasis on the main axis that is the main aim of this study, using the polarization filter made above they can be expressed by the next equation,

$$G_{ij}(t) = G_j(t) \cdot F_j(t) \cdot D_i(t),$$
$$(i=R,T,Z,\ j=1,2,\cdots\cdots,M) \quad \cdots\cdots (6)$$

[7] In addition the component of the incident direction estimated from a part of the primary wave and the direction of the incident angle in parallel together with the component of the SV wave that is at right angles with the incident angle are determined. Thus, P wave and S wave of the earthquakes which emphasizes the above components are synthesized and a figure is drawn. Using this, it becomes possible to symplify wave form discrimination.

## 3. POLARIZATION ANALYSIS TOGETHER WITH WAVE FORM DISCRIMINATION

Here, using a polarization filter actual earthquake records are analyzed. The strong motion records of the Loma Prieta Earthquake are made by the USGS and the CDMG that set up strong motion seismograghs. These include the records of the ground, base rocks (a partial inter structural recording) three component acceleration waves are selected and 49 sites are chosen, and wave form analysis is carried out on the records. In Table 1, observation stations are assembled in the order of shortness of distance from the epicenter. The larger value of the maximal acceleration amp-

Table 1. Name of stations, distance from each site to the epicenter and maximal acceleration of ground motion.

| | Station Code | Station Name | Distance (km) | Maximum Acc.(gal) |
|---|---|---|---|---|
| 01 | COR | Corralitos - Eureka Canyon Rd. | 6.86 | 617.7 |
| 02 | CPI | Capitola - Fire Station | 9.73 | 462.9 |
| 03 | SNT | Santa Cruz - UCSC/Lick Lab. | 10.56 | 433.1 |
| 04 | LLA | Lexington Dam - Left Abutment | 19.05 | 433.0 |
| 05 | LCL | Lexington Dam - Left Crest | 19.05 | 384.3 |
| 06 | LRC | Lexington Dam - Right Crest | 19.05 | 441.0 |
| 07 | SAR | Saratoga - Aloha Ave. | 27.43 | 494.5 |
| 08 | GST | Gilroy - 2st. H. C. Bldg. | 27.81 | 279.7 |
| 09 | G1R | Gilroy 1 - Gavilan College, VT | 28.33 | 433.6 |
| 10 | GGR | Gilroy - Gavilan College, PSB | 28.68 | 349.1 |
| 11 | G2R | Gilroy 2 - Hwy 101/Bolsa Rd. M. | 29.47 | 344.2 |
| 12 | CLA | Coyote Lake Dam - SW Abutment | 30.51 | 471.0 |
| 13 | CDW | Coyote Lake Dam - Downstream | 30.64 | 174.7 |
| 14 | G3R | Gilroy 3 - Gilroy Sewage Plant | 31.09 | 531.7 |
| 15 | G4R | Gilroy 4 - San Ysidro School | 32.00 | 407.9 |
| 16 | GGR | Gilroy 6 - San Ysidro | 35.17 | 166.9 |
| 17 | HAL | Halls Valley - Grant Park | 36.25 | 128.4 |
| 18 | G7R | Gilroy 7 - Mantelli Ranch | 39.58 | 314.3 |
| 19 | ASH | Agnew - Agnew State Hospital | 40.23 | 163.1 |
| 20 | SLI | Salinas - John & Work Street | 46.15 | 110.2 |
| 21 | HOL | Hollister - South St.,Pine Dr. | 47.92 | 361.9 |
| 22 | MOT | Monterey - City Hall | 49.26 | 68.5 |
| 23 | SGO | Sago South - Hollister, C. Rd. | 53.57 | 70.7 |
| 24 | FRE | Fremont - Mission San Jose | 54.60 | 117.7 |
| 25 | WOS | Woodside - Fire Station | 54.71 | 79.7 |
| 26 | AP9 | Crystal Springs Reservoir - S. | 62.56 | 100.9 |
| 27 | AP2 | Crystal Springs Reservoir - P. | 62.89 | 153.6 |
| 28 | FOS | Foster City - Redwood Shores | 64.84 | 277.6 |
| 29 | HCS | Hayward - CSUH Stadium Grounds | 70.48 | 82.6 |
| 30 | HMU | Hayward - Muir School | 70.92 | 160.5 |
| 31 | HBT | Hayward - BART Station | 72.39 | 154.9 |
| 32 | SFI | San Francisco - I. Airport | 79.31 | 325.8 |
| 33 | SSF | South San Francisco - Sierra P. | 83.60 | 102.7 |
| 34 | DIA | San Francisco - Diamond Heights | 91.79 | 110.8 |
| 35 | G2A | Oakland - 2st. Office Bldg. | 91.80 | 238.3 |
| 36 | PIE | Piedmont - P. Jr. High Grounds | 92.49 | 81.2 |
| 37 | OVA | Oakland - Outer Harber Wharf | 94.43 | 281.4 |
| 38 | RIN | San Francisco - Rincon Hill | 94.79 | 88.5 |
| 39 | FST | San Francisco - 18st. C. Bldg. | 95.42 | 157.1 |
| 40 | YBI | Yerba Buena Island | 95.55 | 65.8 |
| 41 | PAC | San Francisco - Pacific Heights | 96.51 | 60.2 |
| 42 | TEL | San Francisco - Telgraph Hill | 96.65 | 90.5 |
| 43 | TRI | Treasure Island | 97.55 | 155.8 |
| 44 | PRE | San Francisco - Presidio | 97.96 | 194.0 |
| 45 | BER | Berkeley - Lawrence Berkeley Lab. | 98.52 | 114.4 |
| 46 | CLI | San Francisco - Cliff House | 99.34 | 105.7 |
| 47 | PTB | Point Bonita | 103.56 | 71.4 |
| 48 | RIC | Richmond - City Hall Parking Lot | 107.55 | 122.7 |
| 49 | OLE | Olema - Point R. R. Station | 137.77 | 157.9 |

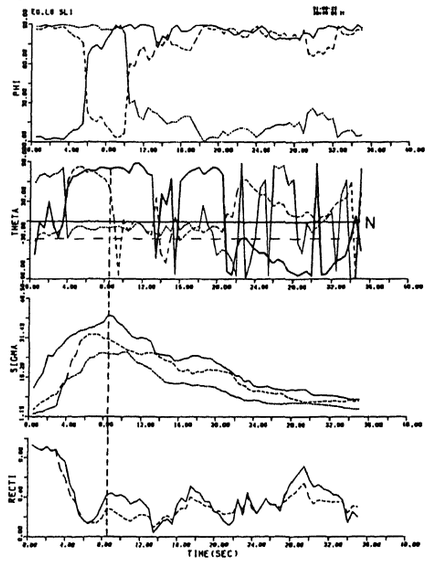


Figure 3. The time course change of incident angle, azimuth, power and rectilinearity of the principal axis(station : Salinas J.W.S.)

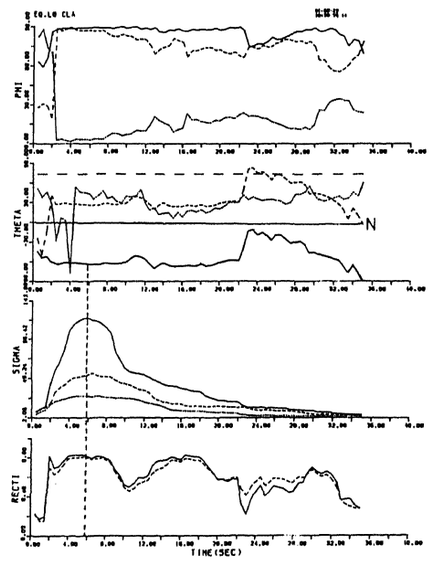


Figure 4. The time course change of incident angle, azimuth, power and rectilinearity of the principal axis(station : Coyote Lake A.B.)

litude of the two horizontal waves is indicated. The analysis includes the behavior;

①The incident angle, the directional azimuth angle of the principal axis of the ground motion( major, intermediate and minor) are calculated.

②The power of principal axis of ground motion are calculated.

③The rectilinear characters which indicate the drawing of the orbit, envelope, and elliptic sphere are investigated.

Figure 3 is one example, analysis from the records at Salinas at 46 km south, south, east from the earthquake epicenter on the Pacific Plate side. At stage [3] and [4], the eigen value of the covariance matrix, the power of principal axes $\lambda$ obtained by the eigen vector , and incident angle $\phi$ together with angle of azimuth $\theta$ are determined. The time course of the incident angle, the azimuth angle the power and the rectilinearity of the principal axis are shown. The maximum values are given by the solid line and the intermediate and the minimum values are shown by the broken line and the dotted line.

Since the incident angle is against the vertical angle, the fact that the main quake motion of the principal axis for maximal and intermediate axis at each station is approximately 90° indicates that a horizontal motion is dominant. The next azimuth is the abcissa co-ordinate and expresses the N direction. From here in the upward direction clockwise + angle, in downward direction - angle is taken. The direction of the horizontal broken line is the direction of observation site drawn between the epicenter and -27.3° N.

In addition, in the figure below $\lambda_1$, $\lambda_2$ and $\lambda_3$ appear to show the time course change of the power of the earthquake motion, the maximal amplitude of 8.5 seconds as compared with the intermediate, and minimal principal axis power have comparatively large amplitudes: This seems to indicate that it shows a ground motion very close to sphere. Compared to this at the outset up to three seconds the amplitude is close to a straight line. The intensity may be expressed as rectilinearity shown on the bottom and is expressed as the ordinate from 0 sphere to 1 a straight line. On the other hand, in the case of Coyote Lake which lies to east, north, east, of the epicenter, in this case of major axis record the direction is constant, and the rectilinearity of maximal amplitude is large, 1.8 and the direction is close to a straight line which can be read in seismic motion.

Table 2 shows the power and the direction of maximal principal axis together with the epicenter and direction of each station. The respective angles from the north and are expressed as the minus angles counter clock wise. When viewed closely the direction of major axis direction and the angles of the direction of epicenter is in most cases aproximately 90°. Further, the value of rectilinearity of the main quake motion is expressed.

Table 2. At the observation stations the maximal axis and power together with the direction and rectilinearity.

| | Station Code | Major Axis Power[1] | Major Axis Direction[2] | Epicenter Direction | Recti-linearity | Amplitude Ratio[3] |
|---|---|---|---|---|---|---|
| 01 | COR | 189.4 | - 18.9° | 84.3° | 0.37 | 1.06 N |
| 02 | CPI | 194.7 | - 7.6° | - 138.8° | 0.29 | 1.01 N |
| 03 | SNT | 166.5 | - 33.7° | - 105.1° | 0.53 | 1.20 N |
| 04 | LLA | 184.9 | 43.1° | 18.8° | 0.75 | 1.37 N |
| 05 | LCL | 237.2 | 44.5° | 18.8° | 0.81 | 1.40 N |
| 06 | LRC | 244.8 | 22.7° | 18.8° | 0.87 | 1.08 N |
| 07 | SAR | 123.4 | 83.3° | - 29.2° | 0.17 | 1.01 E |
| 08 | CST | 80.4 | 89.9° | 97.1° | 0.34 | 1.00 E |
| 09 | G1R | 144.3 | 71.6° | 105.2° | 0.48 | 1.05 E |
| 10 | GGR | 104.2 | 89.7° | 105.0° | 0.41 | 1.00 E |
| 11 | G2R | 128.8 | 45.7° | 102.8° | 0.41 | 1.40 E |
| 12 | CLA | 120.0 | - 63.3° | 73.5° | 0.80 | 1.12 E |
| 13 | CDW | 73.6 | - 39.0° | 72.2° | 0.61 | 1.28 N |
| 14 | G3R | 152.0 | 48.4° | 100.9° | 0.46 | 1.34 E |
| 15 | G4R | 109.6 | 71.1° | 96.9° | 0.38 | 1.06 E |
| 16 | GGR | 67.0 | 68.0° | 92.5° | 0.57 | 1.08 E |
| 17 | WAL | 46.3 | - 35.8° | 23.9° | 0.23 | 1.23 N |
| 18 | G7R | 104.6 | - 53.5° | 91.1° | 0.62 | 1.24 E |
| 19 | ASH | 61.1 | 21.7° | - 9.1° | 0.48 | 1.08 N |
| 20 | SLI | 38.5 | 81.4° | 152.2° | 0.49 | 1.01 E |
| 21 | HOL | 142.3 | - 2.5° | 116.4° | 0.77 | 1.00 N |
| 22 | MOT | 24.2 | 36.4° | - 178.2° | 0.39 | 1.24 N |
| 23 | SGO | 31.5 | 36.7° | 126.6° | 0.52 | 1.25 N |
| 24 | FRE | 47.5 | - 49.9° | - 3.6° | 0.59 | 1.31 E |
| 25 | WOS | 40.0 | 47.3° | - 37.7° | 0.74 | 1.30 E |
| 26 | AP9 | 43.9 | 50.8° | - 40.9° | 0.60 | 1.29 E |
| 27 | AP2 | 49.0 | 22.2° | - 37.2° | 0.62 | 1.08 N |
| 28 | FOS | 123.8 | 89.5° | - 28.6° | 0.61 | 1.00 E |
| 29 | HCS | 28.2 | - 85.9° | - 13.1° | 0.30 | 1.00 E |
| 30 | HMU | 59.5 | - 3.8° | - 14.6° | 0.49 | 1.00 N |
| 31 | HBT | 58.4 | - 50.6° | - 14.6° | 0.42 | 1.29 E |
| 32 | SFI | 102.3 | 53.1° | - 35.3° | 0.57 | 1.25 E |
| 33 | SSF | 29.0 | 21.4° | - 32.5° | 0.42 | 1.07 N |
| 34 | DIA | 41.6 | 26.5° | - 32.0° | 0.53 | 1.12 N |
| 35 | 02A | 77.5 | - 77.4° | - 21.9° | 0.45 | 1.02 E |
| 36 | PIE | 26.4 | 89.0° | - 19.7° | 0.66 | 1.00 E |
| 37 | OWA | 107.3 | - 24.5° | - 24.0° | 0.59 | 1.10 N |
| 38 | RIN | 27.4 | 60.2° | - 28.1° | 0.49 | 1.15 E |
| 39 | FST | 59.6 | 10.2° | - 28.8° | 0.49 | 1.02 N |
| 40 | YBI | 21.7 | 77.8° | - 26.4° | 0.68 | 1.02 E |
| 41 | PAC | 27.0 | - 54.8° | - 30.2° | 0.65 | 1.22 E |
| 42 | TEL | 30.6 | - 88.3° | - 29.0° | 0.52 | 1.00 E |
| 43 | TRI | 65.6 | 77.9° | - 26.5° | 0.78 | 1.02 E |
| 44 | PRE | 53.9 | 84.1° | - 31.4° | 0.50 | 1.01 E |
| 45 | BER | 40.2 | - 71.9° | - 19.3° | 0.79 | 1.05 E |
| 46 | CLI | 38.4 | - 87.7° | - 34.1° | 0.41 | 1.00 E |
| 47 | PTB | 32.4 | - 73.0° | - 33.1° | 0.38 | 1.05 E |
| 48 | RIC | 48.5 | 43.2° | - 22.3° | 0.54 | 1.37 N |
| 49 | OLE | 59.8 | - 39.1° | - 35.9° | 0.55 | 1.29 N |

1) Values of the major axis power lead forth from the three component acceleration digital data.
2) The direction of the major axis and the angle where the case is counter clock wise against N is expressed.
3) Against the maximal acceleration of the original wave the maximal acceleration of major axis component is expressed by the amplitude ratio.

When the surface is viewed, records of such structures as dam sites show large values exceeding 0.6, this clearly indicates straight line behavior. As against this the direction of non clear ground motion which show characteristics close to spheres appear more frequently near the observation stations, then the value of rectilinearity are under 0.4.

In addition the rows on the right hand side as against the original wave, an increase in amplitude ratio is seen in the amplitude of the component wave in the direction of the major axis. The component wave of direction of the major axis, stage [6] of Figure 1 is the radial component surmised, based on the polarization filter analysis, and/or the wave form changed from transverse component that is at right angles with the above. Since among the main ground motion major axis $\lambda_1$ of the wave of the maximal amplitude of the direction can be obtained, the original wave in that direction can be changed and synthesized, it can be said that it is the maximal component wave of the ground motion here.

Therefore, the amplitude of the original wave form becomes somewhat larger. The magnification ratio of the original NS or EW wave would be expressed as such.

The direction alone of the major axis is indicated on the map as in Figure 5. The position of the main shock is indicated by ▲.

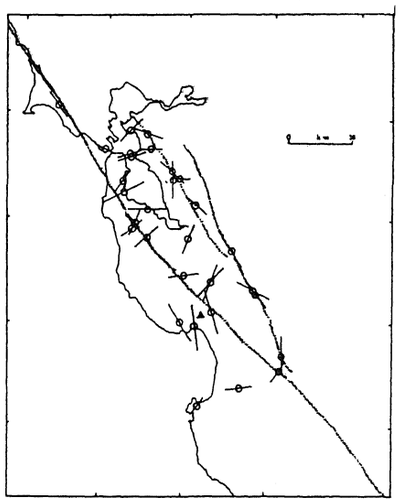

Figure 5. The direction of the major axis is indicated on the map.

It is visually seen at right angles in the wave front direction. As seen in Figure 6, the broken line indicates the spread of wave front that arises from the region of after shock, and is seen clearly as it propagates from the SH wave and the Love wave.

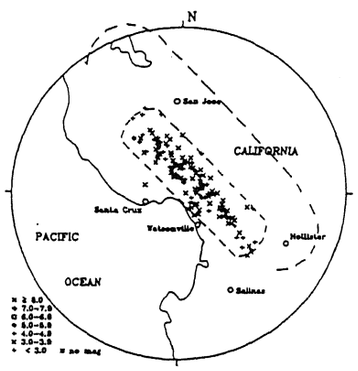


Figure 6. Earthquake epicenters in the Santa Cruz Mountains area (by Preliminary Determination of Epicenters, NEIC).

On the other hand, the characteristics of rectilinearity are indicated elliptic spheres coming from particle orbit in ground motion as shown in Figure 7, map. As naturally expected, near the epicenter since the amplitude is larger, a large elliptic sphere can be formed. Since it is the area adjacent to

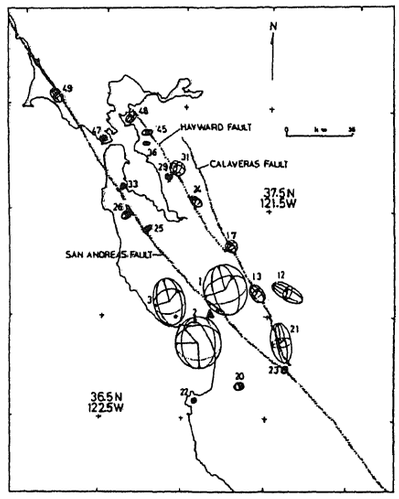


Figure 7. The characteristics of rectilinearity are indicated elliptic spheres coming from particle orbit in ground motion.

the epicenter while it forms an elliptic sphere, as it gradually departs from the epicenter, the direction of ground motion becomes clear and assumes a close to straight line motion causing an increase of the elliptic spheres.

The orbit spectra is studied in order to see whether the dispersive surface wave could be seen. For instance in Figure 8 and Figure 9, the records of Hayward - Muir School (HMU) located at 71km from the epicenter are viewed. Figure 8 is the orbit spectrum of two components from NS-EW. The N direction is taken near the top of the ordinate and the direction is taken at the E direction of the abcissa. At 1.6 second intervals one orbit is completed and horizontally 25 individuals are recorded for 40 seconds. Perpendicularly up to 0.25 Hz～1.50 Hz are analyzed, with 18 lines standing side by side. The top 2 wave

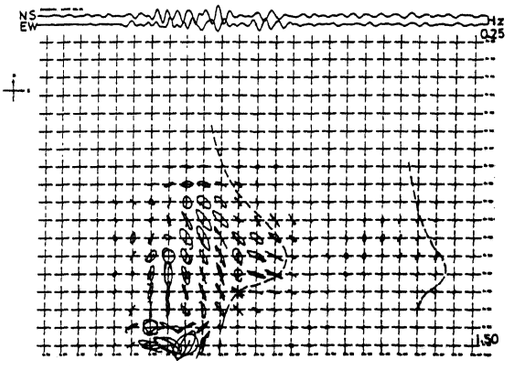


Figure 8. The orbit spectrum of two components from NS-EW.

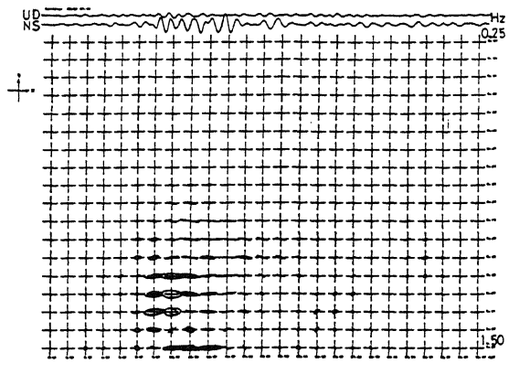


Figure 9. The orbit spectrum of two components from UD-EW.

forms are the NS, EW wave forms in the low frequency region. The same as in Figure 9, this is the orbit spectrum derived from UD-EW component. Carefully comparing the 2 figures , orbits of the same types are selected and the wave forms are drawn. The dispersion of the waves on the left main portion are mostly the shift to Love waves from the dominant SH waves which leaned towards horizontal motion. This indicates that SH waves at phase of main quake motion excelled. Further, the small wave group seen in the right later phase, based on the fact that the vertical component is considerably large, it can be surmised that a shift from SV waves to Rayleigh waves is presented.

## 4. CONCLUSIONS

The method using the polarization has been used since old times. But because it is a procedure of averaging the movement in a time domain, it does not have the power to manipulate the frequency domain and and as a result in the field of engineering the frequency of use is not so large. Even in the time domain , with special regards to the characteristics of the polarized direction obtained by polarization analysis and the special characteristics of particle orbits that characterize the elliptic sphere in the three dimension, by using a digital filter, the earthquake motion can be considered spatially, and thereby conduct a wave analysis. This is how the strength of this method can be brought to bear. From the analyses of the strong motion of Loma Prieta Earthquake, it can be clearly said that

① : the main ground motion of the earthquake is dominated by right angles to the direction of the region of the hypocenter.

② : As the site of the station departed from the hypocenter, the main ground motion of the earthquake showed that SH wave excelled.

③ : As the station departed from the region of the hypocenter, the waves become dispersive , and surface waves such as Love wave and Rayleigh wave are recognized.

④ : Near the main shock the value of rectilinearity became small and the direction became vague.

## ACKNOWLEDGEMENT

The writers wish to acknowledge with deep gratitude the good will of Professor Armen Der Kiureghian of the University of California, in making it possible to gain access to the strong motion earthquake records and data.

Further, we are greatly indebted to the valuable assistance given by Mr. Osamu Nakano, head of the Civil Engineering Research Institute, Structural Research Division, of the Hokkaido Development Bureau.

## REFERENCES

Bolt, B.A. 1990. The mechanism and size of the San Andreas Fault source of the 17 October 1989 earthquake. Proc. Putting the Pieces Together, The Loma Prieta Earthquake One Year Later. San Francisco.

Flinn, E.A. 1965. Signal analysis using rectilinearity and direction of particle motion. Proc. of the IEEE: 1874-1876.

Griffin, J.N. 1966. Application and development of polarization (REMODE) filters. Seismic Data Lab. Report 141, Teledyne Inc. Alexandria.

Huang, M.J., Cao T.Q., Vetter U.R. & A.F. Shakal 1989. Plots of the processed data for the interim set of 14 records from the Santa Cruz Mountains ( Loma Prieta ) Earthquake of 17 October 1989. CSMIP(California Strong Motion Instrumentation Program) , CDMG (California Department of Conservation Division of Mines & Geology).

Huang, M.J., Cao T.Q., Vetter U.R. & A.F. Shakal 1990. Second interim set of CSMIP processed strong-motion records from the Santa Cruz Mountains (Loma Prieta ) Earthquake of 17 October 1989. CDMG.

Huang, M.J., Cao T.Q., Vetter U.R. & A.F. Shakal 1990. Third interim set of CSMIP processed strong-motion records from the Santa Cruz Mountains (Loma Prieta ) Earthquake of 17 October 1989. CDMG.

Kaneko, T. & N. Watanabe 1982. Multiple filter orbit analysis of seismograms. Proc. 6th Japan Earthq. Eng. Symp: 409-416. Tokyo.

Montalbetti, J.F & E.R. Kanasewich 1970. Enhancement of teleseismic body phases with a polarization filter. Geopys. J. R. Aster. Soc. 21:119-129.

National Earthquake Information Center 1989. Preliminary determination of epicenters, Monthly listing. U.S. Department of the Interior/Geological Survey.

Seed, R.B., et al. 1990. Preliminary report on the principal geotechnical aspects of the October 17, 1989 Loma Prieta Earthquake. Report No. UCB/EERC 90-05.